Accepted manuscript doi:
10.1680/jgele.20.00124

Submitted: 09 September 2020

Published online in 'accepted manuscript' format: 01 December 2020

Manuscript title: Episodic direct simple shear tests to measure changing strength for whole-life geotechnical design

Authors: N.I. Laham*, K.A. Kwa*, D.J. White* and S.M. Gourvenec*

Affiliation: *University of Southampton, Southampton, UK

Corresponding author: K. A. Kwa, University of Southampton, Southampton, SO17 1BJ, UK.

E-mail: k.a.kwa@soton.ac.uk

Accepted manuscript doi:
10.1680/jgele.20.00124

Abstract

This technical note describes a set of Direct Simple Shear (DSS) tests that characterise the evolving geotechnical properties of a soft soil, through a loading history that represents episodic loading and consolidation periods as encountered by some offshore infrastructure. The interpretation uses a critical state soil mechanics (CSSM) framework. CSSM provides the necessary building blocks to quantify the balance between undrained cyclic loading and the associated increases in pore pressure, and drainage and consolidation, leading to strength regain. The results show how DSS tests can characterise the through-life response of soft clays. The measured responses showed the changing strength of the clay due to consolidation effects following loading, and match predictions from simple models. The results show how DSS tests can characterise the types of behaviour also seen in centrifuge models and field penetrometer tests related to the long term response of soft clays under offshore infrastructure.

Keywords: Offshore engineering; Whole-life; Geotechnics; Direct simple shear tests; Clays

Accepted manuscript doi:
10.1680/jgele.20.00124

INTRODUCTION

Offshore infrastructure for renewable energy and oil and gas production is subjected to a range of actions from metocean and operational conditions. These actions are transmitted via structures, mooring lines or pipelines to foundation or anchoring systems. These loads can affect the geotechnical properties of the seabed and in turn affect the capacity and response of the infrastructure over its lifetime (Gourvenec 2020). Whole-life geotechnical design couples the life cycle of imposed actions with the evolving geotechnical resistance, to forecast the soil-structure response across the design life of the infrastructure. It is essential to reliably estimate the changing available seabed resistance and stiffness throughout the whole-life of the structure to predict its response and optimally design and manage the asset. Transient, sustained, cyclic or episodic actions can affect the strength, stiffness and consolidation parameters of the seabed leading to variations in 'current' seabed resistance and the system reliability over the whole-life of the structure. Allowing for these changes can have a beneficial design outcome, offering opportunities for more efficient systems including reductions in foundation or anchoring size, reduced risk of fatigue, greater insight for late life management and informed decommissioning processes for offshore infrastructure (Gourvenec 2020).

It is well recognised that sustained monotonic compressive loading can improve geotechnical resistance through consolidation while undrained cyclic loading may reduce resistance through cyclic softening. Models for both cases are well established in engineering practice (e.g. Schofield & Wroth 1968, Andersen 2015). The strength and stiffness of soft soils is also affected by consolidation during continuous cyclic loading of sufficiently long duration, and by episodic loading that involves cyclic loads with intervening consolidation. Such loading could be caused by intervals of bad weather or by operating cycles such as heating and cooling of pipelines. In soft clay, these processes generally increase the subsequent undrained strength and stiffness. Whole-life effects of changing soil properties have been observed during flow round penetrometer tests (Hodder et al. 2013, Cocjin et al. 2014; O'Loughlin et al, 2017), interface shear tests (Boukpeti & White 2017), and large scale laboratory tank tests and geotechnical centrifuge tests of pipelines, sliding foundations (Smith & White, 2014, Cocjin et al. 2014, 2017, Han et al. 2016; Zhou et al 2019; Lai et al., 2020) and pile foundations (Bayton et al, 2018; Richards et al, 2018, 2019; Abadie et al., 2019; Truong et

al., 2019). Applications and impact of whole-life geotechnical design are summarised in Gourvenec 2018 and Gourvenec 2020.

For wider application of whole-life geotechnical design to offshore geotechnical infrastructure, a more accessible, cost-effective and established method of characterising whole-life geotechnical responses is necessary, beyond the model testing example above. This technical note explores the potential for characterising evolving geotechnical properties – strength, stiffness and consolidation parameters – through extended direct simple shear (DSS) tests. The DSS test is commonly used in offshore geotechnical site investigation due to smaller required sample size compared to triaxial testing, and because it produces an intermediate soil strength between triaxial compression and extension which is appropriate if a single measured value is to be used for foundation capacity assessment (Mayne, 1985; Kinner & Ladd 1973; Randolph, 2000).

EXPERIMENTAL DETAILS

Direct simple shear apparatus

A suite of DSS tests was performed at the University of Southampton using a GDS Instruments 10kN electromechanical dynamic cyclic simple shear (EMDCSS) apparatus. This DSS apparatus has two linear actuators controlling vertical movement of the loading ram, and horizontal movement at the base of the sample. These linear actuators are connected to displacement transducers and load cells via a feedback loop, enabling displacement- and load-controlled testing. Teflon-coated, stainless steel stacked rings surround the specimen to impose a zero lateral strain boundary condition.

The apparatus deformation and lateral confinement system were calibrated immediately prior to the test program and all vertical displacements and shear stresses have been corrected based on these calibrations in agreement with ASTMD6528-07 (ASTM, 2007). A GDS pressure controller was used to measure pore water pressures in the sample, connected via drainage holes in the top and bottom platens. The pressure controller and lines were flushed and refilled with de-aired water before each test to ensure minimal air was present in the system.

Specimen preparation and assembly

Reconstituted kaolin, with properties listed in Table 1, was prepared as a slurry at a water content twice the liquid limit and mixed under a vacuum for 24 hours before being transferred to a 105mm diameter tube and consolidated in increments to a maximum vertical

stress of 60kPa. This stress level was chosen to target the minimum strength that is practical for sample preparation and to give soil strengths representative for shallow soft clay

The stress increments were applied for 12 hours and the final increment was applied for at least 24 hours. Individual specimens were extruded from the tubes of consolidated kaolin and trimmed to size using a round, 100mm diameter and 27mm tall cutter. The specimens were pressed out of the sample cutter into the removable base of the DSS, where the metal stacked rings and rubber membrane had already been assembled. The base was gently placed and secured in the bottom of the DSS apparatus. The top of the DSS was lowered until the top platen was just touching the top of the sample. A small vertical stress (<1kPa) was applied as seating pressure and the settlements were monitored overnight to ensure the sample was no longer settling before the consolidation stage commenced. This displacement was included in the calculation of the final specimen height. Finally, the rubber membrane was pulled up and sealed with O-rings around the top and bottom platens.

Testing programme and procedure

Table 2 summarises the tests performed. The test labels indicate whether they were monotonically (M) or episodically (E) sheared, and include the consolidated vertical effective stress and for the episodic tests, the applied shear stress ratio, relative to the average strength ratio measured from the two monotonic tests ($\frac{s_u}{\sigma'_{v0}} = 0.255$). The specimens were reconsolidated in the DSS apparatus following the procedure set out in ASTMD6528-07 (ASTM, 2007). Consolidation was performed at 0.1kPa/min which ensured minimal pore pressure build-up within the sample.

The monotonic tests were performed under displacement control at a rate of 0.1mm/min to assess the monotonic DSS strength in normally consolidated conditions. The applied stress path and cyclic shear loading procedure adopted in the episodic cyclic tests are illustrated in Figure 1 and consisted of 6 episodes of undrained half-cycles with intervening consolidation stages, followed by a final monotonic, undrained shear stage (half cycle 7) to failure.

The episodic tests were performed under stress control, at a rate of 0.1kPa/min. The target shear stresses spanned a range of fractions of the monotonic strength, representative of soil elements close to an episodically-loaded structure. Constant height conditions were applied during the shearing stages in both monotonic and episodic tests to ensure constant sample volume, according to the method outlined in Dyvik et al (1987).

During the episodic consolidation stages, the vertical stress was returned to the original consolidation stress, drainage was then allowed and the volume of water that flowed out of the sample was measured via the pressure controller. Sample settlement was monitored and was typically complete within an hour. Finally, the undrained shear stage to failure was controlled at a displacement rate of 0.1mm/min.

RESULTS

Shearing response

The effective stress paths during monotonic tests M62 and M90 in Figure 2a show a rise in pore water pressure as the effective stress falls, and the state moves to the critical state line (CSL). Similar stress paths were followed in the first half cycle of the episodic tests (Figures 2b, c, and d). With further episodes of consolidation and shearing, the build-up in pore water pressure decreased, similar to the idealised effective stress path shown in Figure 1.

The episodic test E63-0.67 shown in Figure 2b, failed at a higher shear stress, and denser state than the monotonic test M62 with same initial conditions, demonstrating the gain in strength with episodes of undrained shear and consolidation. The final undrained strengths achieved in E72-0.70 and E75-0.48 were greater than M90, with the intervening consolidation stage in these cyclic tests eclipsing the higher consolidation stress in M90.

Volumetric response

The changes in effective vertical stress during shear and the changes in void ratio during consolidation both decreased with each subsequent episode of undrained shear and consolidation (Figure 3). This reflects the sample becoming denser, stiffer and experienced smaller increases in pore pressure, due to a reducing tendency to contract.

Stiffening from each cycle of shear and consolidation was also observed in the volumetric and shear strains, which decreased with each episode, as shown in Figures 4 and 5.

As samples compressed and stiffened, updated values of the coefficient of consolidation, c_v, were quantified for each intervening stage of consolidation, as shown per half cycle in Figure 6, normalised using c_v/c_{v0} where c_{v0} was obtained after the first half cycle of loading. These values of c_v are calculated using the Taylor root time method from the settlement response during each reconsolidation stage (Taylor, 1948). The largest increase in c_v occurred from episode 1 to episode 2, when the samples experienced the largest volume strains and increase in stiffness. An implication of this trend is that changes in strength due to this type of episodic loading will happen at an increasing rate, due to the faster consolidation rate

following each cycle of shear and consolidation. A rate of consolidation estimated using the initial value, c_{v0}, would underestimate the effect.

Calculated change in undrained strength

Three methods for predicting the ratio between the undrained strength before ($s_{u,i}$) and after ($s_{u,i+1}$) an episode of shearing and consolidation have been compared with the test results. Method 1 uses the measured changes in void ratio according to Equation 1 (Schofield & Wroth, 1968):

$$\frac{s_{u,i+1}}{s_{u,i}} = \exp\left(\frac{e_i - e_{i+1}}{\lambda}\right) \qquad \text{Eq1}$$

Method 2 uses the measured pore pressures and a construction in e vs σ'_v space (Figure 7) from Yasuhara et al., (1991):

$$\frac{s_{u,i+1}}{s_{u,i}} = \frac{\sigma'_{v,fi+1}}{\sigma'_{v,fi}} = \left(\frac{\sigma'_{v,i+1}}{\sigma'_{v,i}}\right)^{\frac{\kappa}{\lambda}} = \left(\frac{\sigma'_{v0}}{\sigma'_{v0} - \Delta u_i}\right)^{\frac{\kappa}{\lambda}} = \left(\frac{1}{1 - \frac{\Delta u_i}{\sigma'_{v0}}}\right)^{\frac{\kappa}{\lambda}} \qquad \text{Eq2}$$

A limitation of methods 1 and 2 is that the DSS test results are inputs. Method 3 avoids this limitation by applying Eq2 with an assumed effective stress path that varies with OCR: see Appendix for derivation (Yasuhara et al., 1994). This prediction method can therefore be validated or calibrated from test results, then applied to more general input loading conditions, including successive cycles of varying amplitude.

The predicted increases in undrained strength with each half cycle from methods 1, 2 and 3 were similar and the predicted undrained strength of the sample was within a few percent of the actual undrained strength achieved during half cycle 7 (Figure 8), for example using Method 3 the predicted gain in s_u/s_{u0} is always within 7%. The small variations between the predicted and actual strengths may be a result of the natural variability in the material properties, or due to inhomogeneities developing at the sample boundaries at large strains (>20%) (Airey et al. 1985, 1987), which were particularly noticeable in tests E72-0.70 and E75-0.48 and in the slight variation in stress paths between tests M62 and M90.

The results show consistent patterns of increasing undrained strengths during episodic loading as a result of the intervening consolidation stages, where drainage is permitted and samples become denser and stiffer. This behaviour is consistent with a simple CSSM-type predictive model, as well as the existing literature on the evolving properties of soft soils when subjected to loading conditions relevant to the whole-life response of offshore

foundations (Gourvenec, 2018, 2020). Therefore, this DSS testing procedure is capable of characterising the evolving geotechnical properties and strengthening of soft soils.

CONCLUDING REMARKS

This technical note presents the results from episodic DSS tests on reconsolidated soft clay, where each cycle consists of an undrained shear stage and a consolidation stage. These loading conditions are relevant to in-service conditions for a variety of offshore infrastructure, including shallow foundations, monopiles and plate anchors, and for a range of design approaches, including traditional factor of safety (FoS), tolerable mobility or performance-based design. The results showed that the strength, stiffness and consolidation coefficient of the clay increased due to consolidation effects that followed shear stages. These trends are consistent with observations from centrifuge models and field penetrometer tests representing the whole-life response of geotechnical offshore infrastructure. The DSS testing procedure, with benefits including small sample sizes, shorter consolidation times, and the ability to apply complex stress histories, can capture the evolving geotechnical properties in these conditions, and a simple predictive model can capture the observed changes in strength.

ACKNOWLEDGEMENTS

The work presented in this paper is supported through the Royal Academy of Engineering Chair in Emerging Technologies in Intelligent & Resilient Ocean Engineering, the EPSRC Supergen Offshore Renewable Energy Hub (EP/S000747/1) and the Erasmus Mundus Scholarship Programme. The authors are also grateful to Mr Harvey Skinner, Geomechanics Laboratory Manager at the National Infrastructure Laboratory, University of Southampton, and Dr Fernando Alvarez Borges, for their technical assistance during the laboratory testing.

APPENDIX

Figures A1 and A2 show the parameters used.

Calculation of strength and definitions of OCR

Initially, the sample is K_0 normally consolidated such that

$$\sigma'_{vc} = \sigma'_{v0} = \sigma'_{ve} \qquad \text{A1}$$

More generally, these values differ when the over consolidation ratio (OCR) ≠ 1. The undrained strength is then given by

$$s_u = R\sigma'_{ve} \qquad \text{A2}$$

Where R is the normally consolidated undrained strength ratio, determined from a test at OCR=1. A value of R=0.27 is used in Figure 8. The current OCR prior to shearing is defined treating the K_0 consolidated line as the normally consolidated line (NCL)

$$OCR = \frac{\sigma'_{vc}}{\sigma'_{v0}} \qquad \text{A3}$$

Following Yasuhara et al. (1994), a quasi-OCR can be defined along a constant volume line as

$$OCR_q = \frac{\sigma'_{ve}}{\sigma'_{v0}} \qquad \text{A4}$$

Using the quasi-OCR, the current strength can always be written as

$$s_u = R\sigma'_{ve} = R\ OCR_q\ \sigma'_{vo} \qquad \text{A5}$$

The different definitions of OCR are related by geometry of the unload-reload and critical state lines with gradients κ and λ (Ladd et al., 1974; Ladd, 1991; Mayne et al., 2009)

$$OCR_q = OCR^{1-\kappa/\lambda} = OCR^{\Lambda} \qquad \text{A6}$$

where $\Lambda = 1 - \kappa/\lambda$ and is 0.7-0.95 for most soils.

Calculation of pore pressure generated in response to a shear stress

The vertical effective stress at failure is taken to be:

$$\sigma'_{vf} = \frac{s_u}{tan\phi'} \qquad \text{A7}$$

which is a common approach with the shear strength being at the top of the Mohr's circle (Carraro et al., 2017).

The pore pressure generated during shearing to failure is:

$$\Delta u_{max} = \sigma'_{v0} - \sigma'_{vf} = \sigma'_{v0} - \frac{s_u}{tan\phi'} \qquad \text{A8}$$

Combining A8 with A2 and A4, the following expression results

$$\frac{\Delta u_{max}}{\sigma'_{v0}} = 1 - \frac{R\ OCR_q}{tan\phi} \qquad \text{A9}$$

The pore pressure generated during shearing towards failure is a fraction of Δu_{max} that depends on the shape of the stress path, which can be defined by

$$\frac{\Delta u_i}{\Delta u_{max}} = \left(\frac{\tau_{mob}}{s_u}\right)^{\beta} \qquad \text{A10}$$

Where $\beta > 1$ (Cocjin et al., 2017). A value of $\beta = 1.5$ was used in Figure 8, selected via fitting β to the monotonic test data and predicted increases in s_u using Methods 1 and 2.

Calculation of the change in strength due to pore pressure dissipation

To calculate the change in strength from a cycle of pore pressure generation and dissipation, only OCR_q needs to be updated because σ'_{v0} is constant between cycles. Therefore, s_u can be calculated according to A6, A7 and A8. Furthermore, the change in void ratio during the dissipation phase can be expressed as

$$\Delta e = -\kappa ln\left(\frac{\sigma'_{v0}-\Delta u_i}{\sigma'_{v0}}\right) = -\kappa ln\left(1-\frac{\Delta u_i}{\sigma'_{v0}}\right) \text{ and } \Delta e = \lambda ln\left(\frac{\sigma'_{ve,i+1}}{\sigma'_{ve,i}}\right) \quad \text{A11}$$

Therefore,

$$\frac{\sigma'_{ve,i+1}}{\sigma'_{ve,i}} = \left(1-\frac{\Delta u_i}{\sigma'_{v0}}\right)^{-\kappa/\lambda} = \left(1-\frac{\Delta u_i}{\sigma'_{v0}}\right)^{\Lambda-1} \quad \text{A12}$$

Equation A12 allows the quasi-OCR to be updated

$$\left(OCR_q\right)_{i+1} = \left(OCR_q\right)_i \times \frac{(\sigma'_{ve})_{i+1}}{(\sigma'_{ve})_i} = \left(OCR_q\right)_i \times \left(1-\frac{\Delta u_i}{\sigma'_{v0}}\right)^{-\kappa/\lambda} \quad \text{A13}$$

and the updated undrained strength can be calculated from A5. The fractional increase in undrained strength can now be expressed as

$$\frac{s_{u,i+1}}{s_{u,i}} = \left(1-\frac{\Delta u_i}{\sigma'_{v0}}\right)^{-\kappa/\lambda} \quad \text{A14}$$

LIST OF SYMBOLS

c_v coefficient of consolidation
c_{v0} initial coefficient of consolidation
e void ratio
e_0 initial void ratio
e_{cs} void ratio on critical state line at $\sigma'_v = 1$kPa
e_f final void ratio
G_s specific gravity of solid fraction
M critical state friction constant
s_u undrained strength
s_{u0} monotonic undrained strength
s_u/σ'_{v0} strength ratio
Δu_i change in pore water pressure during a particular undrained shear stage
γ shear strain
ϵ_v volumetric strain
κ slope of swelling line
λ slope of normal compression line
ϕ' angle of internal friction
σ'_v vertical effective stress
σ'_{v0} equilibrium vertical effective stress
τ shear stress
τ/σ'_{v0} shear stress ratio
τ_{mob} mobilised shear stress
τ_{mob}/σ'_{v0} applied shear stress ratio

REFERENCES

Abadie, C. N., Byrne, B. W. & Houlsby, G. T. (2019). Rigid pile response to cyclic lateral loading: laboratory tests. Géotechnique 69, No. 10, 863–876, https://doi.org/10.1680/jgeot.16.P.325.

Airey, D. W., Budhu, M., & Wood, D. M. (1985). Some aspects of the behaviour of soils in simple shear. In P. K. Banerjee, & R. Butterfield (Eds.), Developments in soil mechanics and foundation engineering: Vol. 2: Stress-strain modelling of soils (pp. 185-213).

Airey, D. W., & Wood, D. M. (1987). An evaluation of direct simple shear tests on clay. Géotechnique, 37(1), 25-35.

Andersen K.H. (2015) Cyclic soil parameters for offshore foundation design. The 3rd McClelland Lecture. Proc. 3rd Intnl Symp. Frontiers in Offshore Geotechnics, Oslo, Norway, 5 – 82, ISBN: 978-1-138-02848-7

Bayton, S. M., Black, J. A. & Klinkvort, R. T. (2018). Centrifuge modelling of long term cyclic lateral loading on monopiles. In Physical modelling in geotechnics – ICPMG 2018 (eds A. McNamara, S. Divall, R. Goodey, N. Taylor, S. Stallebrass and J. Panchal), pp. 689–694. London, UK: CRC Press.

Boukpeti N., & White D. J. (2017) Interface shear box tests for assessing axial pipe-soil resistance. Géotechnique, 67(1):18-30. http://dx.doi.org/10.1680/jgeot.15.P.112

Carraro, J. A. H. (2017). Analysis of simple shear tests with cell pressure confinement. Geomechanics and Geoengineering, 12(3), 169-180.

Cocjin M., Gourvenec S., White D.J and Randolph M.F. (2014) Tolerably mobile subsea foundations – Observations of performance. Géotechnique 64(11): 895-909. http://dx.doi.org/10.1680/geot.14.P.098

Cocjin M., Gourvenec S., White D.J & Randolph M.F. (2017) Theoretical framework for predicting the response of tolerably mobile subsea installations. Géotechnique 67(7): 608-620 http://dx.doi.org/10.1680/jgeot.16.P.137

Dyvik R., Berre T., Lacasse S & Raadim B. (1987) Comparison of truly undrained and constant volume direct simple shear tests Géotechnique 37, no 1 p 3 -10

Gourvenec S. (2018) The role of centrifuge modelling on capturing whole-life response for optimization of offshore foundation design. Keynote. Proc. 9th International Conference on Physical Modelling in Geotechnics, ICPMG, London. Taylor and Francis. p. 51-75.

Gourvenec S. (2020) Whole-life geotechnical design: What is it? What's it for? So what? And what next? Proc. 4th International Symposium on Frontiers in Offshore Geotechnics. (Delayed to) 8 – 11 November 2021, Proceedings published Aug 2020. Austin, Texas, USA, ASCE Geo-Institute and DFI

Han, C., Wang, D., Gaudin, C., O'Loughlin, C.D. & Cassidy, M.J., (2016). Behaviour of vertically loaded plate anchors under sustained uplift. Géotechnique, 66(8), pp.681-693.

Hodder M.S., White D.J. & Cassidy M.J. (2013) An effective stress framework for the variation in penetration resistance due to episodes of remoulding and reconsolidation. Géotechnique 63(1):30–43

Ladd C.C. & Foot R. (1974) New Design Procedure for Stability of Soft Clays, Journal of the Geotechnical Engineering Division Vol 100, GT7, p 763 786

Ladd C.C. (1991) Stability Evaluation during Staged Construction, Journal of Geotechnical Engineering, Vol 117 No 4, p 540-615, 22nd Karl Terzaghi lecture

Lai Y., Wang L., Hong Y. & He B. (2020) Centrifuge modeling of the cyclic lateral behavior of large-diameter monopiles in soft clay: Effects of episodic cycling and reconsolidation. Ocean Engineering, 200, 2020, 107048,

Mayne, P.W. (1985). A review of undrained strength in direct simple shear. Soils and Foundations 25 (3): 64-72

Mayne P.W., Coop M.R., Springman S.M. & Huang A. (2009) Geomaterial behavior and testing, State of the Art lecture in: proceeding of the 17th Int Conf on Soil Mechanics and Geotechnical engineering, ICSMGE vol 4. Millpress /IOS Rotterdam

Randolph, M.P., (2000). Effect of strength anisotropy on capacity of foundations Developments in Theoretical Geomechanics, Smith & Carter (eds), 2000 Balkema, Rotterdam

Richards, I. A., Byrne, B. W. & Houlsby, G. T. (2018). Physical modelling of monopile foundations under variable cyclic lateral loading. In Physical modelling in geotechnics – ICPMG 2018

Richards I.A., Byrne B.W. & Houlsby G.T. (2019) Monopile rotation under complex cyclic lateral loading in sand. Géotechnique. Ahead of print https://doi.org/10.1680/jgeot.18.P.302

Taylor, D.W. (1948) Fundamentals of Soil Mechanics, John Wiley and Sons, New York.

Truong, P., Lehane, B. M., Zania, V. & Klinkvort, R. T. (2019). Empirical approach based on centrifuge testing for cyclic deformations of laterally loaded piles in sand. Géotechnique 69, No. 2, 133–145, https://doi.org/10.1680/jgeot.17.P.203.

Schofield, A., & Wroth, P. (1968). Critical state soil mechanics. McGraw-hill.

Smith V. B. & White D. J. (2014) Volumetric hardening in axial pipe soil interaction. In Proc. Offshore Technology Conference Asia, OTC ASIA 2014: Meeting the Challenges for Asia's Growth (Vol. 2, pp. 1611-1621).

Yasuhara, K., & Andersen, K. H. (1991). Recompression of normally consolidated clay after cyclic loading. Soils and Foundations, 31(1), 83-94.

Yasuhara, K. (1994). Postcyclic undrained strength for cohesive soils. Journal of Geotechnical Engineering, 120(11), 1961-1979.

Zhou, Z., O'Loughlin, C. D., White, D. J., & Stanier, S. A. (2019). Improvements in plate anchor capacity due to cyclic and maintained loads combined with consolidation. Géotechnique, 1-18.

Accepted manuscript doi:
10.1680/jgele.20.00124

Table 1: Characteristics of kaolin clay

Property	**Value**
Liquid Limit LL (%)	61
Plastic Limit PL (%)	27
Specific Gravity G_s	2.7
Void ratio at σ_v'=1kPa on critical state line e_{cs}	2
Slope of normal consolidation line λ	0.17
Slope of swelling line κ	0.032
Angle of internal friction ϕ' (degrees)	24

Table 2: Summary of DSS tests

Test Name	Initial void ratio e_0	Final void ratio, e_f	Applied vertical consolidation stress, $\boldsymbol{\sigma'_{v0}}$ (kPa)	Applied cyclic stress ratio $\frac{\tau_{mob}}{\sigma'_{v0}}$	Final strength ratio $\frac{s_u}{\sigma'_{v0}}$	Vertical effective stress at failure (kPa)	Final undrained strength, s_u (kPa)
M62	1.38	1.29	62	-*	0.24	32.6	14.9
M90	1.35	1.24	90	-*	0.27	56.6	24.2
E63-0.67	1.36	1.20	63	0.17	0.35	50.2	21.8
E72-0.70	1.37	1.18	72	0.18	0.36	58.2	25.7
E75-0.48	1.36	1.17	75	0.12	0.40	70.8	30.3

*Monotonic tests

List of figure captions

Accepted manuscript doi:
10.1680/jgele.20.00124

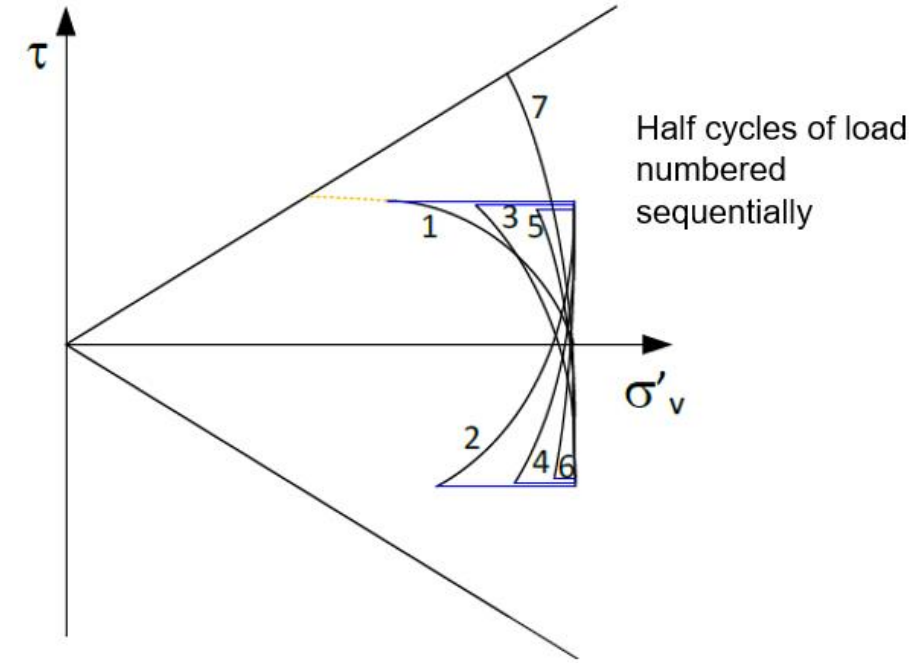

(a)

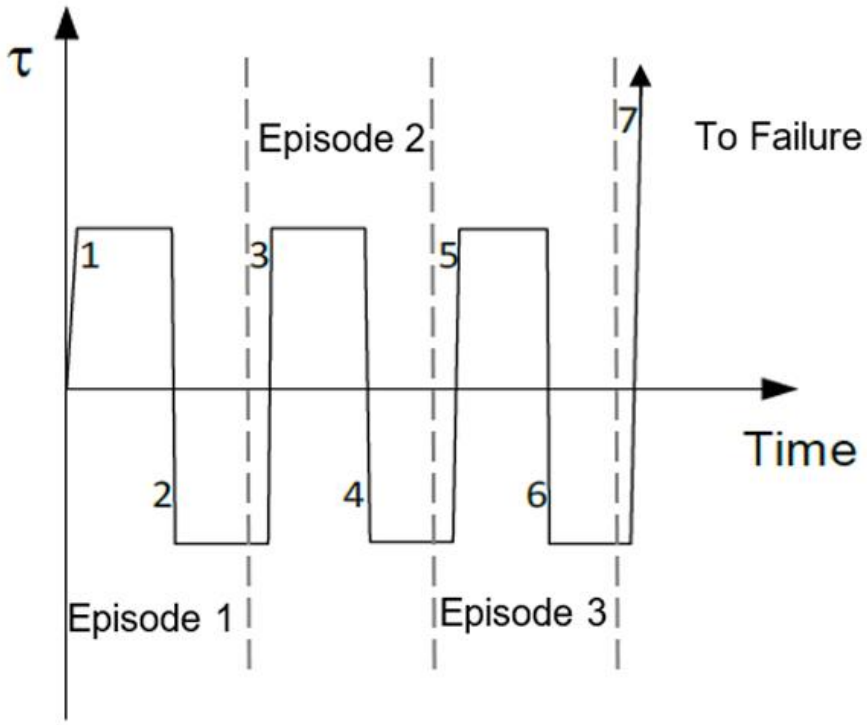

(b)

Figure 01

Accepted manuscript doi:
10.1680/jgele.20.00124

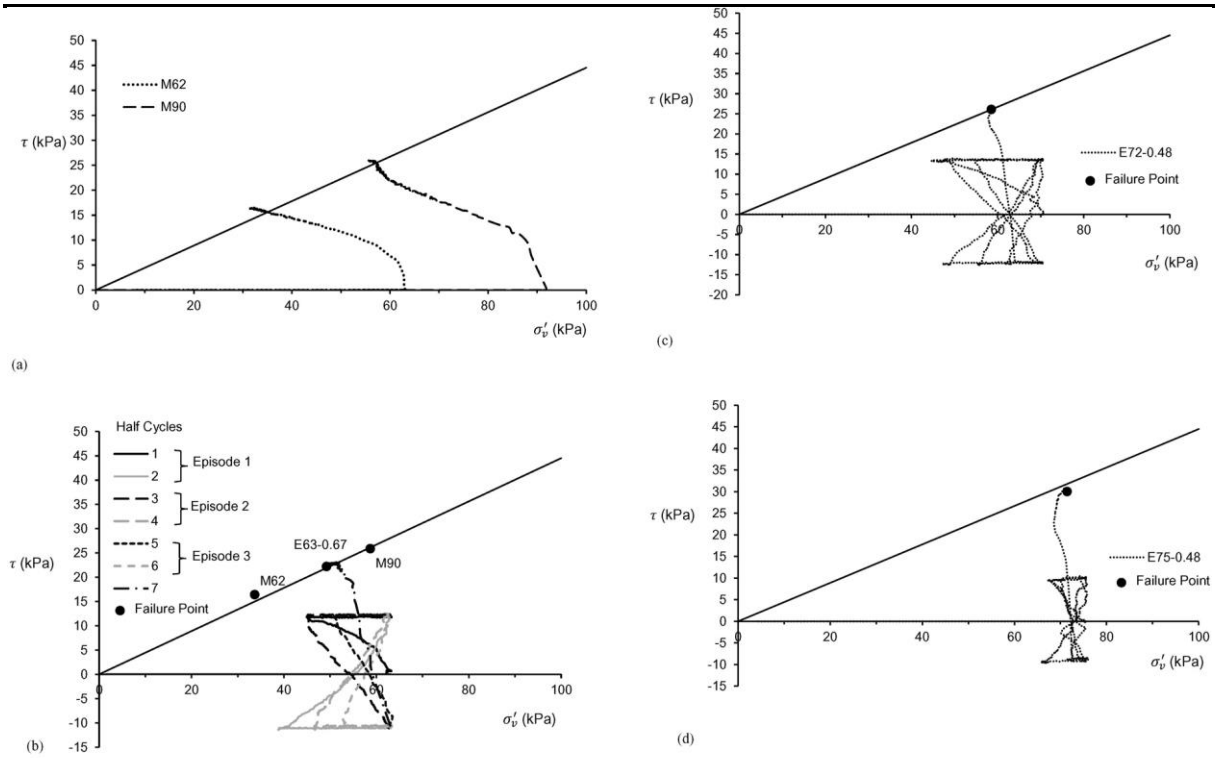

Figure 2: Effective stress paths for (a) monotonic tests and (b), (c), (d) episodic tests

Accepted manuscript doi:
10.1680/jgele.20.00124

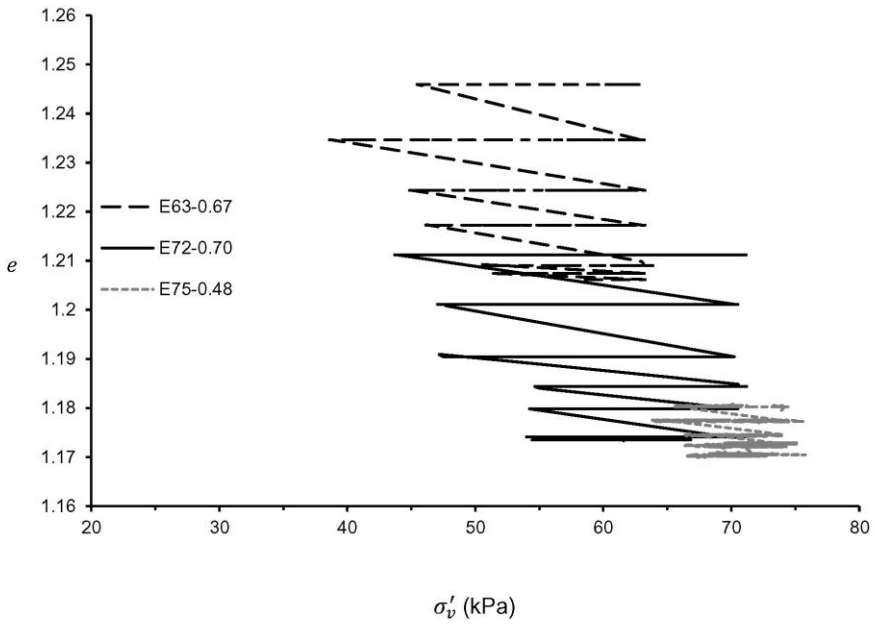

Figure 3: Change in volume due to shear and consolidation for varying initial states and applied shear stresses

Accepted manuscript doi:
10.1680/jgele.20.00124

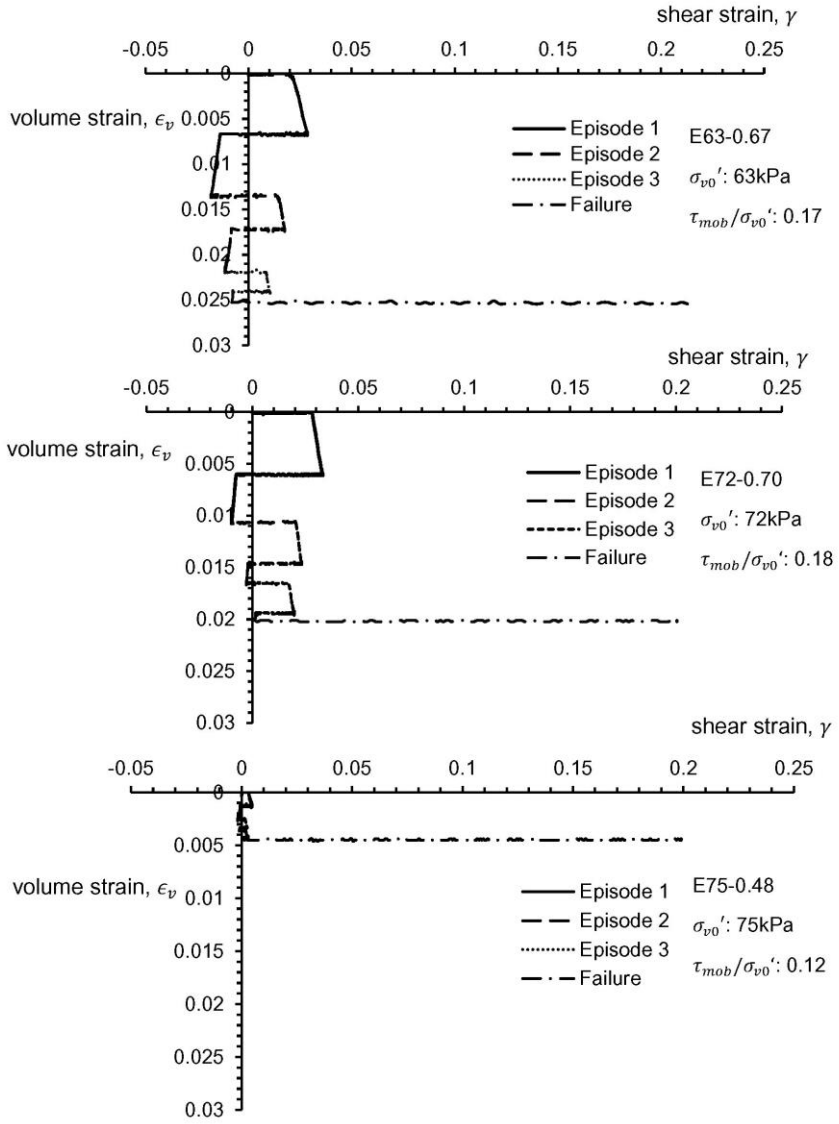

Figure 4: Evolution of compressibility and stiffness for episodically sheared samples (a) E63-0.67, (b) E72-0.70 and (c) E75-0.48

Accepted manuscript doi:
10.1680/jgele.20.00124

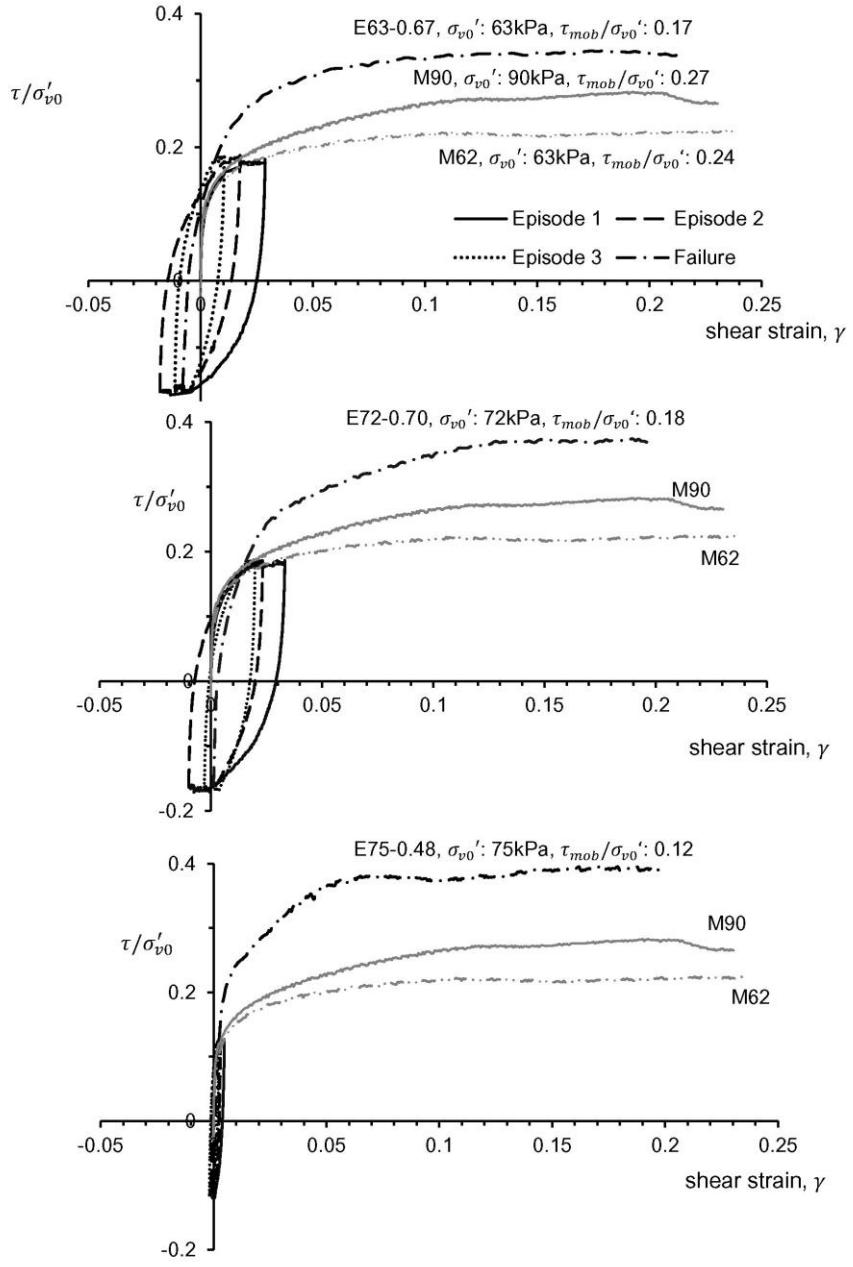

Figure 5: Comparison of stress-strain behaviour between monotonically and episodically sheared samples (a) E63-0.67, (b) E72-0.70 and (c) E75-0.48

Accepted manuscript doi:
10.1680/jgele.20.00124

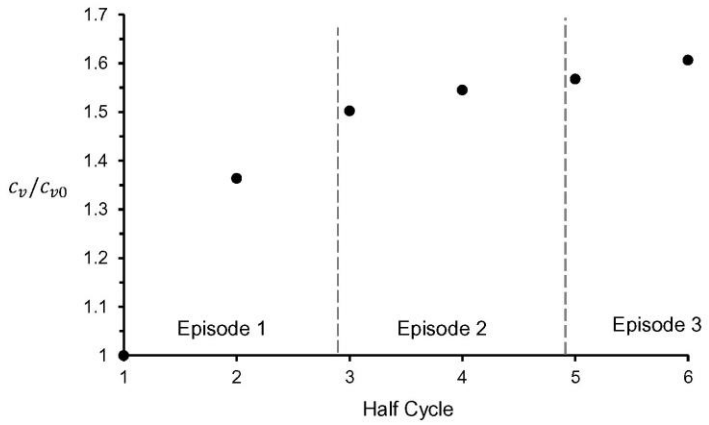

Figure 6: Normalised evolution of consolidation coefficient (c_v) (test E72-0.48)

Accepted manuscript doi:
10.1680/jgele.20.00124

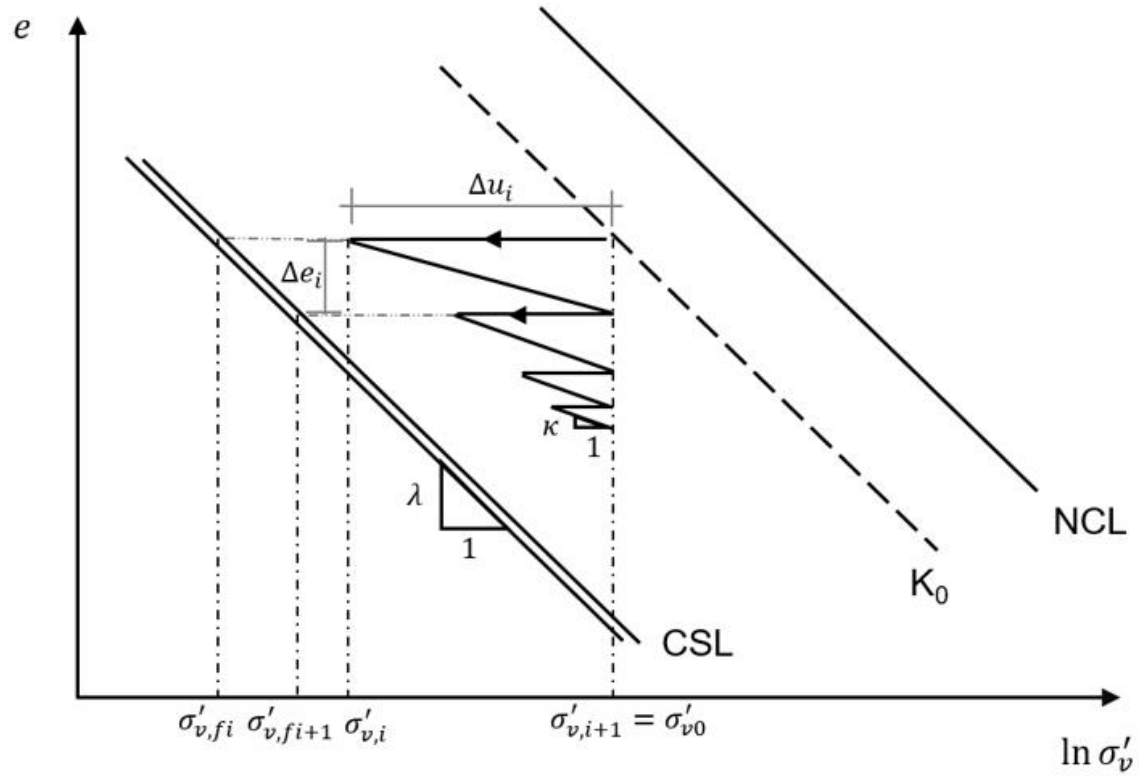

Figure 07

Accepted manuscript doi:
10.1680/jgele.20.00124

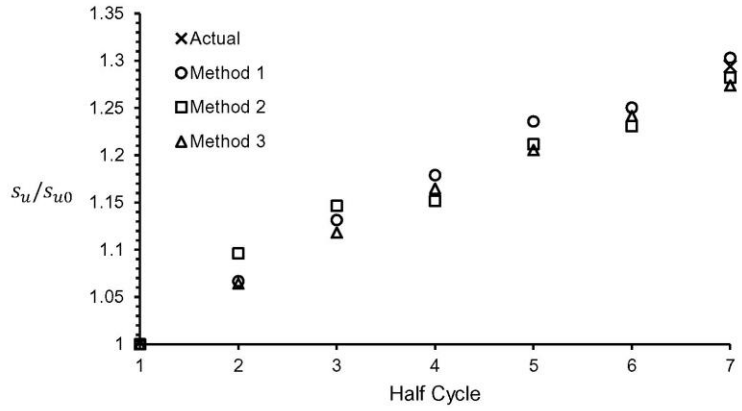

(a)

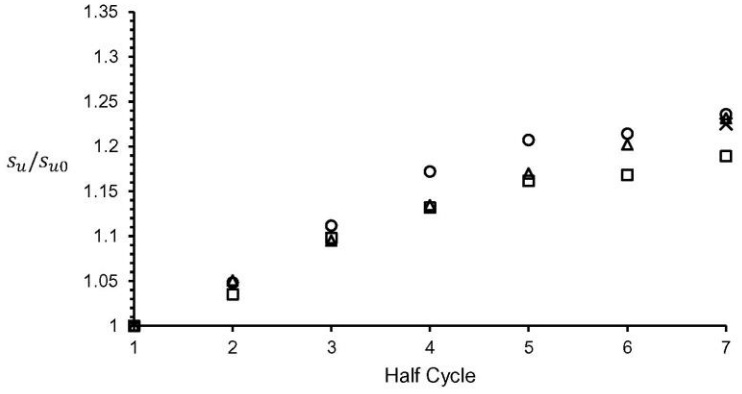

(b)

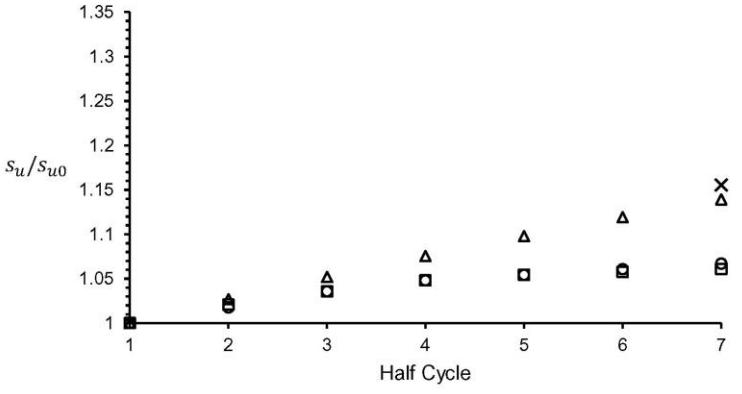

(c)

Figure 8: Predicted and measured gains in undrained strength (a) E63-0.67, (b) E72-0.70 and (c) E75-0.48

Accepted manuscript doi:
10.1680/jgele.20.00124

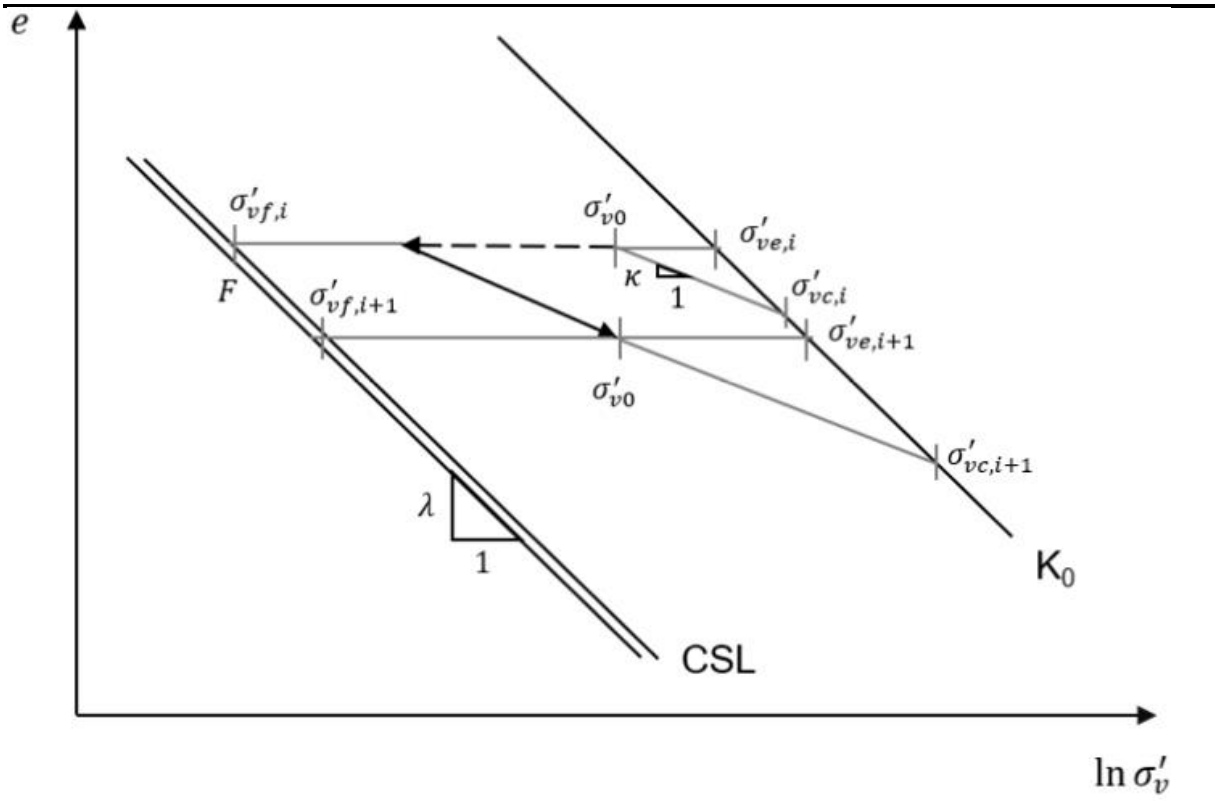

Figure A1

Accepted manuscript doi:
10.1680/jgele.20.00124

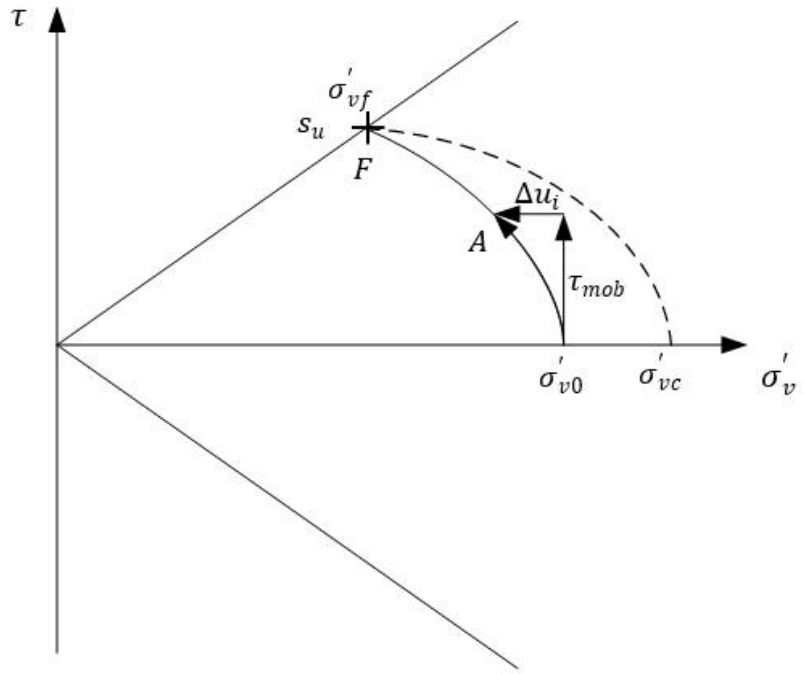

Figure A2